In Silico Model for Tumor Diagnosis based on Bloodstream Penetrating Extracellular Vesicles

Mohammad Zoofaghari[1,2],Martin Damrath[3], Mladen Veletić[2,3], Krizia Sagini[2,4], Jacob Bergsland[2], Alicia Llorente[2,4,5], Ilangko Balasingham[2,3]

[1]Yazd University, Yazd, Iran, [2]Oslo University Hospital, Oslo, Norway, [3]Norwegian University of Science and Technology, Trondheim, Norway, [4]University of Oslo, Oslo, Norway, [5]Oslo Metropolitan University, Oslo, Norway

ABSTRACT

During the last decade, extracellular vesicles (EVs) have emerged in the scientific community because of their potential as natural drug nanocarriers and biomarkers in disease diagnosis, especially for cancer. While a few studies have focused on the propagation and biodistribution of tumor-derived EVs within the extracellular space or the bloodstream, there is a lack of simultaneous consideration of the transport of EVs within the blood vessels, surrounding tissue and tumor microenvironment. Here, we introduce an *in silico* model that simulates the release of EVs from cancer cells, their transport within the surrounding tissues, uptake into the bloodstream, and circulation within the segment of the blood vessels network comprising the arterial, capillary and venous vessels. By examining the obtained simulation results, we also propose a novel diagnostic procedure for sub-millimeter tumors based on the EV penetration rate into the circulatory system. Our simulations demonstrate the sensitivity of the approach to tumor size, whereas our findings further demonstrate that EVs offer a promising avenue for non-invasive disease diagnosis.

CCS CONCEPTS

• **Applied computing** → **Systems biology**.

NANOCOM '23, September 20–22, 2023, Coventry, United Kingdom

ACM ISBN 979-8-4007-0034-7/23/09…$15.00
https://doi.org/10.1145/3576781.3608719

KEYWORDS

Extracellular vesicles, *in silico* modeling, cancer diagnosis, biomarkers.

ACM Reference Format:
Mohammad Zoofaghari[1,2],Martin Damrath[3], Mladen Veletić[2,3], Krizia Sagini[2,4], Jacob Bergsland[2], Alicia Llorente[2,4,5], Ilangko Balasingham[2,3] . 2023. In Silico Model for Tumor Diagnosis based on Bloodstream Penetrating Extracellular Vesicles. In *10th ACM International Conference on Nanoscale Computing and Communication (NANOCOM '23), September 20–22, 2023, Coventry, United Kingdom.* ACM, New York, NY, USA, 7 pages. https://doi.org/10.1145/3576781.3608719

1 INTRODUCTION

Extracellular vesicles (EVs) are lipid-bound particles ranging in size from 30 nm to 5 µm, which are typically released by cells into the extracellular space [9]. EVs are attracting more and more attention from scientists as they play an important role in intercellular communication. By encapsulating their cargo, typically lipids, nucleic acids, and proteins, they protect them from enzymes and can even overcome some of the stringent extracellular and intracellular barriers [1]. By combining their biological durability, natural targeting property, and phagocytosis-inhibition factors with their specific cargo [19], EVs offer a promising pathway towards diagnosis as biomarkers, and therapy as natural drug nanocarriers of diseases, especially for cancer [9].

In addition to propagating within tissues, EVs can also enter the bloodstream and be further transported into tissues. This bears great potential for non-invasive disease diagnosis and drug delivery which also prompted the establishment of mathematical models for the EV propagation in the bloodstream [12]. Understanding the propagation of EVs within tissues and the bloodstream is essential for developing and optimizing diagnostic and drug delivery systems. Besides costly and invasive *in vivo* and unrealistic *in vitro* experiments, mathematical models and simulations offer a cost-effective *in silico* alternative to bring light into the darkness while reducing the need for experiments.

An overview of the main propagation mechanisms of particles in extracellular space is given in [22]. A three-dimensional model for the *in silico* determination of interstitial fluid flow and intratumorally-injected nanoparticle distribution is developed in [16]. The authors realize the model in COMSOL Multiphysics software and investigate the influence of nanoparticle size, transvascular transport, vascular normalization, and the presence of a necrotic core. When it comes to the propagation of EVs, there is only a limited amount of work involving mathematical modeling. A mathematical model for the propagation of tumor-derived EVs in the bloodstream is established in [12], which is fitted to experimental data. The transport of EVs in a tumor microenvironment governed by the interstitial flow and diffusion is simulated in [15]. To validate the simulation, the experimental determination of the breast cancer-derived EVs transport in the tumor microenvironment built of macrophages and T cells is investigated. Other relevant works consider the propagation of EVs in extracellular space taking into account the effects such as volume fraction, tortuosity, and anomalous diffusion [21, 25].

There are numerous works on blood flow simulation in the literature. For example, BloodVoyagerS [13] provides a simulation platform for the entire cardiovascular system of the human body. Other works focus on the simulation of the arterial tree [3], the systemic circulation [6], the pulmonary and systemic circulation [4, 10], or the blood flow in the heart, brain, or lungs [23]. Another approach pursues the interpretation and mathematical description of drug delivery systems using the molecular communication paradigm. The examples include a communication model between platelets and endothelial cells in a blood vessel [11], a particle propagation model in a blood vessel accounting for transcytosis across single-layered endothelial cells [2], and a pharmacokinetic model for the biodistribution of a drug-loaded particle through the blood stream within the body [5].

However, in all these works, there is a lack of detailed simultaneous consideration of the propagation of particles/EVs within the blood vessel, the surrounding tissue, and the transition between these two. In our work, we observe the EV biodistribution in a tumor and surrounding tissue, their uptake into the bloodstream, and their transport within the blood circulatory system. For this purpose, we model the bloodstream through a capillary network consisting of arteriole, capillaries, and venules surrounding the tissues. We focus on the simulation of the EVs released from cancer cells for the purpose of a novel, non-invasive diagnostic procedure for sub-millimeter tumors. This is done based on the temporal behavior of the penetration rate of tumor-derived EVs into the circulatory system, which we find to be different for different tumor sizes. The sensitivity of this approach to the tumor size is evaluated through the simulations.

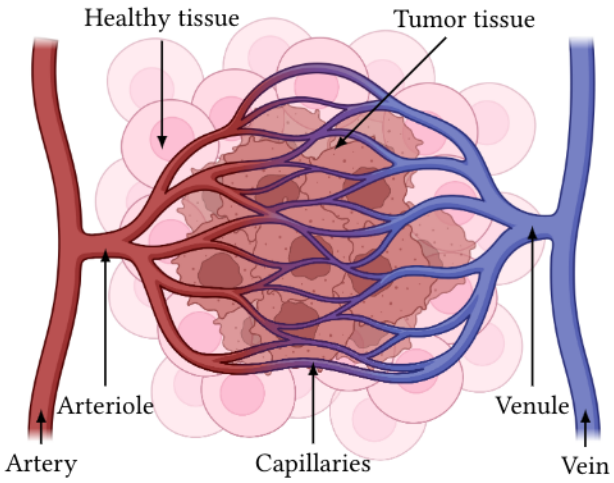

Figure 1: Schematic of blood vessels and the tumor and healthy cells. The illustration is created using BioRender.com

The remainder of this paper is structured as follows. In Section 2, we define a system model for the structure including a blood vessel network and partially cancerous tissue to which expedient boundary conditions and the reaction rates are assigned. In the end, we present in Section 3 results addressing the biodistribution and penetration rate of EVs in the predefined structure and within the bloodstream, respectively, and conclude the paper in Section 4.

2 SYSTEM MODEL

A schematic representation that can reproduce a real scenario in great detail can be found in Fig. 1. In this figure, the sections are distinguished referring to the artery, the vein, the capillary network (Ω_c), the tumor area (Ω_t), and the healthy tissue (Ω_h). Considering the fact that cancer cells need to exchange oxygen and nutrients to survive, the capillary network is expanded throughout the tumor area. EVs produced in the tumor area may pass through the capillary wall into the bloodstream or enter the healthy part of the tissue within the organ. The rate of release of EVs into the blood depends on the permeability of the vessel wall, which is modeled by the permeability coefficient given by

$$k_p = \frac{D_w}{d_w}, \tag{1}$$

where D_w denotes the diffusion coefficient of EVs inside the capillary wall and d_w stands for capillary wall thickness. Due to its thinner wall and higher permeability coefficient compared to the other vessel types, the capillary is more likely to transfer the EVs from the tumor or healthy area into the bloodstream. Here, we set a *diffusion barrier boundary*

Table 1: Default simulation parameters, which are applied throughout the numerical results, if not stated otherwise.

Parameters	Symbol	Value	Unit	Ref.
Arteriole diameter	d_{a}	30	µm	[26]
Capillary diameter	d_{c}	8	µm	[26]
Venule diameter	d_{v}	20	µm	[26]
Arteriole wall thickness	$d_{\mathrm{w,a}}$	20	µm	[18]
Capillary wall thickness	d_{w}	1	µm	[18]
Venule wall thickness	$d_{\mathrm{w,v}}$	2	µm	[18]
Inlet blood velocity in arteriole	u_{a}	1000	µm/s	[26]
Inlet blood velocity in venule	u_{v}	200	µm/s	[26]
Blood viscosity	μ	4.5	cP	[24]
Blood density	ρ	1060	$\mathrm{Kg/m^3}$	[24]
Average diameter of tumor mass	d_{tm}	300	µm	[17]
No. tumor cells	N_t	25000		[8]
Permeability coefficient of capillary wall	k_{p}	4	µm/s	[7]
Diffusion coefficient inside the tumor	D_{t}	10^{-2}	$\mu\mathrm{m^2/s}$	[14]
Diffusion coefficient inside the healthy tissue	D_{h}	16×10^{-2}	$\mu\mathrm{m^2/s}$	[14]
Release rate of tumor-derived EVs	R_{t}	2×10^{-10}	$\mathrm{mol/m^3/s}$	[20]
Release rate of healthy tissue-derived EVs	R_{t}	10^{-10}	$\mathrm{mol/m^3/s}$	[20]

condition to the capillary wall in which k_{p} relates the flow of EVs in the tumor (healthy tissue), $\boldsymbol{J}_{\mathrm{t(h)}}$, and the bloodstream, $\boldsymbol{J}_{\mathrm{c}}$, to the difference of EVs concentration inside the tumor (healthy tissue), $c_{\mathrm{t(h)}}(\boldsymbol{r}, t$, and inside the capillary, $c_{\mathrm{c}}(\boldsymbol{r}, t)$. This condition is given by

$$\hat{\boldsymbol{n}} \cdot \boldsymbol{J}_{\mathrm{t(h)}}(\boldsymbol{r}, t) = k_{\mathrm{p}}(c_{\mathrm{t(h)}}(\boldsymbol{r}, t) - c_{\mathrm{c}}(\boldsymbol{r}, t)), \quad \boldsymbol{r} \in \partial\Omega_{\mathrm{c}}, \tag{2}$$

and

$$\hat{\boldsymbol{n}} \cdot \boldsymbol{J}_{\mathrm{c}}(\boldsymbol{r}, t) = k_{\mathrm{p}}(c_{\mathrm{c}}(\boldsymbol{r}, t) - c_{\mathrm{t(h)}}(\boldsymbol{r}, t)), \quad \boldsymbol{r} \in \partial\Omega_{\mathrm{c}}, \tag{3}$$

respectively, where $\boldsymbol{r} \in \partial\Omega_{\mathrm{c}}$, denotes the position vector of a point in the capillary wall for which $\hat{\boldsymbol{n}}$ is defined as a unit outward directed normal vector. Please note that $\boldsymbol{J}_{\mathrm{t,c}}$ here shows the rates of the particles perpendicularly crossing a unit area. On the other hand, the penetration rate of EVs from the tumor into the healthy area results from the following *partition condition*:

$$c_{\mathrm{h}}(\boldsymbol{r}, t) = k_{\mathrm{t}} c_{\mathrm{t}}(\boldsymbol{r}, t), \quad \boldsymbol{r} \in \partial\Omega_{\mathrm{t}}, \tag{4}$$

where $\partial\Omega_{\mathrm{t}}$ indicates the boundary region of the tumor and k_{t} stands for the partition condition coefficient given by

$$k_{\mathrm{t}} = \sqrt{\frac{D_{\mathrm{t}}}{D_{\mathrm{h}}}}, \tag{5}$$

In (5), D_{t} and D_{h} are the diffusion coefficient of EVs within the tumor and healthy area, respectively. As a matter of fact, k_{p} and k_{t} should be determined empirically through *in vitro* or *in vivo* experiments. However, as we will show in the numerical results, the values given by (1) and (5) could be exploited for the homogeneously modeled diffusive environments (i.e. Ω_{c}, Ω_{t} and Ω_{h}) considered for the current *in silico* simulation.

We also assign a partially absorbing condition to the healthy tissue boundary, $\partial\Omega_{\mathrm{h}}$, expressed as

$$\hat{\boldsymbol{n}} \cdot \boldsymbol{J}_{\mathrm{h}}(\boldsymbol{r}, t) = k_{\mathrm{f}} c_{\mathrm{h}}(\boldsymbol{r}, t), \quad \boldsymbol{r} \in \partial\Omega_{\mathrm{h}}, \tag{6}$$

where k_{f} indicates the forward reaction coefficient on $\partial\Omega_{\mathrm{h}}$ and $\boldsymbol{J}_{\mathrm{h}}(\boldsymbol{r}, t)$ is the EVs flux in the healthy tissue. After the EVs enter the blood, the drift of EVs (which is the dominant factor of particle movement inside the vessel) is acquired by the blood flow velocity within the capillary, $\boldsymbol{u}_{\mathrm{b}}(\boldsymbol{r}, t)$. The advection-diffusion equation which describes the flow of EVs inside the capillaries network is given by

$$\frac{\partial c_{\mathrm{c}}(\boldsymbol{r}, t)}{\mathrm{d}t} + \boldsymbol{u}_{\mathrm{b}}(\boldsymbol{r}, t) \cdot \nabla c_{\mathrm{c}}(\boldsymbol{r}, t) - D_{\mathrm{c}} \nabla \cdot \boldsymbol{J}_{\mathrm{c}}(\boldsymbol{r}, t) + k_{\mathrm{d,c}} c_{\mathrm{c}}(\boldsymbol{r}, t) = R_{\mathrm{c}}(\boldsymbol{r}, t), \tag{7}$$

where D_{c} is the diffusion coefficient of EVs inside the capillary, $k_{\mathrm{d,c}}$ is the degradation coefficient of EVs in the blood, and $R_{\mathrm{c}}(\boldsymbol{r}, t)$ is the rate of EVs released into the blood by a separate source. Here we assume that EVs in the blood are only originated from the tissue, thus $R_{\mathrm{c}}(\boldsymbol{r}, t) = 0$. We know that the red blood cells (RBCs) may shed EVs including both endosome-derived exosomes and plasma-membrane-derived microvesicles (MVs) into the blood resulting in non-zero $R_{\mathrm{c}}(\boldsymbol{r}, t)$ that could be incorporated in the future models. We also have similar equations for the advection-diffusion of EVs in the tumor and healthy areas given by

$$\frac{\partial c_{\mathrm{t}}(\boldsymbol{r},t)}{\mathrm{d}t} + \boldsymbol{u}_{\mathrm{i,t}}(\boldsymbol{r},t)\cdot\nabla c_{\mathrm{t}}(\boldsymbol{r},t) - D_{\mathrm{t}}\nabla\cdot\boldsymbol{J}_{\mathrm{t}}(\boldsymbol{r},t) + k_{\mathrm{d,t}}c_{\mathrm{c}}(\boldsymbol{r},t) = R_{\mathrm{t}}(\boldsymbol{r},t), \quad (8)$$

and

$$\frac{\partial c_{\mathrm{h}}(\boldsymbol{r},t)}{\mathrm{d}t} + \boldsymbol{u}_{\mathrm{i,h}}(\boldsymbol{r},t)\cdot\nabla c_{\mathrm{h}}(\boldsymbol{r},t) - D_{\mathrm{h}}\nabla\cdot\boldsymbol{J}_{\mathrm{t}}(\boldsymbol{r},t) + k_{\mathrm{d,h}}c_{\mathrm{c}}(\boldsymbol{r},t) = R_{\mathrm{h}}(\boldsymbol{r},t), \quad (9)$$

respectively. In (8) and (9), $\boldsymbol{u}_{\mathrm{i,t}}(\boldsymbol{r},t)$ and $\boldsymbol{u}_{\mathrm{i,h}}(\boldsymbol{r},t)$ stand for the interstitial flow and $k_{\mathrm{d,t}}$ and $k_{\mathrm{d,h}}$ indicate the degradation of EVs in the tumor and healthy areas, respectively.

Here we assume that the flow of blood in the capillary network is in the laminar incompressible flow regime where the blood velocity vector is solenoidal (divergenceless). This is the case that we usually observe in the middle of a vessel. Any disruption at vessel walls (e.g. due to atherosclerosis, thrombosis, and emboli) can magnify the turbulent flow representing the underlying pathology. In order to calculate the blood velocity in the vessels, we exploit the Navier–Stokes equation for the conservation of momentum and the continuity equation for the conservation of mass given by

$$\rho\frac{\partial \boldsymbol{u}_{\mathrm{b}}(\boldsymbol{r},t)}{\mathrm{d}t} + \rho\left(\boldsymbol{u}_{\mathrm{b}}(\boldsymbol{r},t)\cdot\nabla\right)\boldsymbol{u}_{\mathrm{b}}(\boldsymbol{r},t) = \nabla p + \nabla\cdot\left(\mu\nabla\boldsymbol{u}_{\mathrm{b}}(\boldsymbol{r},t) + \mu\nabla\boldsymbol{u}_{\mathrm{b}}(\boldsymbol{r},t)^{T}\right), \quad (10)$$

where ρ, p, μ denote the blood density, pressure, and dynamic viscosity, respectively, and $\boldsymbol{q}^{T}$ stands for the transpose of a vector $\boldsymbol{q}$. The vessel walls are assumed to have a no-slip condition with zero blood flow velocity. Moreover, to model the flow of the circulatory system into the capillary network, we set an inlet velocity (i.e. u_{a} for the arteriole and u_{v} for the venule) and an outlet condition (i.e. zero-pressure condition), respectively, to the entry and exit of the arteriole and venule. Penetration rate R_{s} of the EVs into the circulatory system given in mol/s could be derived as a surface integration over the venule cross section (VCS) given by

$$R_{\mathrm{s}} = \iint_{\mathrm{VCS}} c(\boldsymbol{r},t)u_{\mathrm{n}}(\boldsymbol{r},t)\,\mathrm{d}s, \quad (11)$$

where $u_{\mathrm{n}}(\boldsymbol{r},t)$ denotes the component of the blood velocity perpendicular to the VCS calculated from (10). In the next section, we will investigate the effect of various parameters including the tumor size, blood velocity, and the permeability coefficient on R_{s}.

3 NUMERICAL RESULTS

In this paper, we recruit the COMSOL Multiphysics software to solve (7)-(10) subject to the boundary conditions we discussed in the previous section using the finite element method. We exploit *Transport of Diluted Species (TDS)* and *Single-phase Flow (SPF)* toolboxes to simulate the advection-diffusion of EVs in three aforementioned regions and the laminar flow of blood in the capillary network, respectively. The blood velocity obtained from SPF is employed in TDS to calculate the concentration of EVs secreted into the venule. The parameter values for these simulations are listed in Table 1.

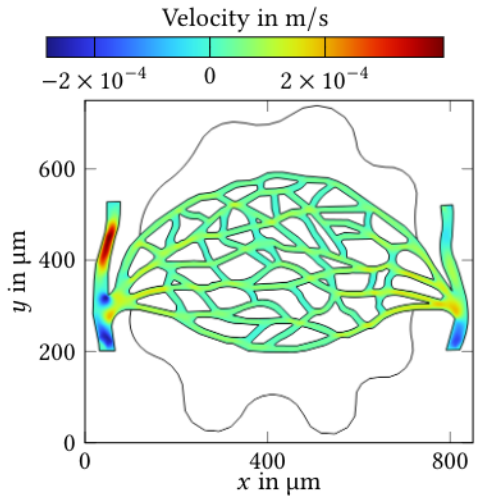

(a) x-component

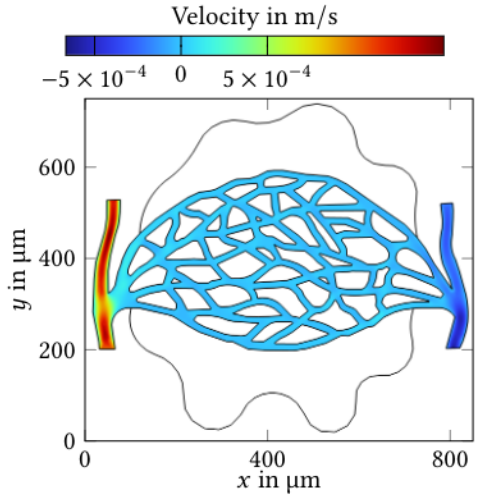

(b) y-component

Figure 2: (a) x- and (b) y-component of blood velocity in the arteriole, capillaries, and venule. The blood inlet is considered at the lower part of the artery and at the higher part of the vein.

Fig. 2 shows the blood velocity at arteriole, capillaries, and venule given by (10). Here we illustrate the velocity's x and y components separately, in which the negative values stand for the blood velocity flowing in the negative direction

of the x- or y-axis. As expected, the blood flow is slow in the capillaries because of the large total cross-sectional area which provides proper EVs exchange at this site.

Here, we assume uniform EV sizes to avoid diffusion dispersion in the current scenario. We address a diagnostic approach for the sub-millimeter tumor sizes. In this scale, we classify small, moderate, and large tumors as illustrated in Fig. 3. The distribution of EVs within the tumor and healthy tissue and capillary network at different time points is shown in Fig. 4 for the small tumor. We see in this figure that EVs accumulate mainly in the tumor parts, as they hardly diffuse there to reach the capillaries. Once the EVs cross the vessel walls, they are immediately transferred into the vein and their concentration in the capillaries decreases rapidly. In this figure, we also show the flux streamlines of EVs from the tissue toward the vein outlet, which, as expected, are magnified as they approach the vein.

In Fig. 5, we also plot R_s versus time for the healthy tissue and various tumor sizes. The cross area is considered somewhere around the venule outlet at $y = 625\,\mu$m to measure R_s given by (11). However, this point is not that critical as we expect to have approximately the same flux at different cross areas. It is clear in the figures that R_s initially rises up to a specified value and almost flattens out after a certain point in time. Obviously, the temporal behavior of the EVs penetration rate within the bloodstream is well distinct for different tumor sizes. The larger tumors decrease the effective diffusion coefficient of the environment resulting in lower R_s. Some other simulation results demonstrate that the thicker capillaries cause the EVs to take longer to cross the vessel wall and the R_s is lower. These modeling results provide a new diagnostic platform to track the tumor progress based on the number of EVs penetrating the circulatory system at a specified time course.

4 CONCLUSION

In this conference paper, we examine *in silico* modeling of the transfer of extracellular vesicles from a cancer tissue to the circulatory system. We used COMSOL Multiphysics to simulate the temporal and spatial biodistribution of EVs in the tissue and their translocation into blood circulation. We divided the considered structure into three regions: the healthy tissue, the tumor tissue, and the capillary network, for which a suitable condition was established at the boundary between the different parts. The obtained results show that the penetration of EVs into the blood vessels is significantly affected by the tumor size. This could be taken into account in the early-stage EV-based cancer diagnosis when tumors are in the sub-millimeter range. In future work, this research should be improved by using three-dimensional models of the tissue capillary structure. The numerically obtained biodistribution results should be validated by experimental data.

REFERENCES

[1] Hamidreza Arjmandi, Hamid Khoshfekr Rudsari, João Santos, Mohammad Zoofaghari, Oleksandr Ievglevskyi, Masamitsu Kanada, Ali Khaleghi, Ilangko Balasingham, and Mladen Veletić. 2021. Extracellular Vesicle-Mediated Communication Nanonetworks: Opportunities and Challenges. *IEEE Communications Magazine* 59, 5 (2021), 68–73. https://doi.org/10.1109/MCOM.001.2000994

[2] Hamidreza Arjmandi, Mohammad Zoofaghari, Seyed Vahid Rouzegar, Mladen Veletic, and Ilangko Balasingham. 2021. On Mathematical Analysis of Active Drug Transport Coupled With Flow-Induced Diffusion in Blood Vessels. *IEEE Transactions on NanoBioscience* 20 (Jan. 2021), 105–115. Issue 1. https://doi.org/10.1109/TNB.2020.3038635

[3] Alberto P. Avolio. 1980. Multi-branched model of the human arterial system. *Medical and Biological Engineering and Computing* 18, 6 (1980), 709–718. https://doi.org/10.1007/BF02441895

[4] Michael Broomé, Elira Maksuti, Anna Bjällmark, Björn Frenckner, and Birgitta Janerot-Sjöberg. 2013. Closed-loop real-time simulation model of hemodynamics and oxygen transport in the cardiovascular system. *BioMedical Engineering OnLine* 12, 1 (2013), 69. https://doi.org/10.1186/1475-925X-12-69

[5] Youssef Chahibi, Massimiliano Pierobon, and Ian F. Akyildiz. 2015. Pharmacokinetic Modeling and Biodistribution Estimation Through the Molecular Communication Paradigm. *IEEE Transactions on Biomedical Engineering* 62 (Oct. 2015), 2410–2420. Issue 10. https://doi.org/10.1109/TBME.2015.2430011

[6] Martin J. Conlon, Donald L. Russell, and Tofy Mussivand. 2006. Development of a Mathematical Model of the Human Circulatory System. *Annals of Biomedical Engineering* 34, 9 (2006), 1400–1413. https://doi.org/10.1007/s10439-006-9164-y

[7] Fitzroy E. Curry. 1979. Permeability coefficients of the capillary wall to low molecular weight hydrophilic solutes measured in single perfused capillaries of frog mesentery. *Microvascular research* 17, 3 (1979), 290–308.

[8] Ugo Del Monte. 2009. Does the cell number 109 still really fit one gram of tumor tissue? *Cell cycle* 8, 3 (2009), 505–506.

[9] Laura M. Doyle and Michael Zhuo Wang. 2019. Overview of Extracellular Vesicles, Their Origin, Composition, Purpose, and Methods for Exosome Isolation and Analysis. *Cells* 8 (July 2019), 727. Issue 7. https://doi.org/10.3390/cells8070727

[10] Bartomiej Fajdek and Alicja Golnik. 2010. Modelling and simulation of human circulatory system. In *15th International Conference on Methods and Models in Automation and Robotics*. IEEE, Miedzyzdroje, Poland, 399–404. https://doi.org/10.1109/MMAR.2010.5587199

[11] Luca Felicetti, Mauro Femminella, Gianluca Reali, Paolo Gresele, Marco Malvestiti, and John N. Daigle. 2014. Modeling CD40-based molecular communications in blood vessels. *IEEE Transactions on NanoBioscience* 13 (Sept. 2014), 230–243. Issue 3. https://doi.org/10.1109/TNB.2014.2340134

[12] Scott Ferguson and Ralph Weissleder. 2020. Modeling EV Kinetics for Use in Early Cancer Detection. *Advanced biosystems* 4 (Dec. 2020), e1900305. Issue 12. https://doi.org/10.1002/adbi.201900305

[13] Regine Geyer, Marc Stelzner, Florian Büther, and Sebastian Ebers. 2018. BloodVoyagerS: Simulation of the Work Environment of Medical Nanobots. In *Proc. ACM Int. Conf. on Nanoscale Computing and Communication (NANOCOM)*. Association for Computing Machinery, New York, NY, USA, Article 5, 6 pages. https://doi.org/10.1145/3233188.3233196

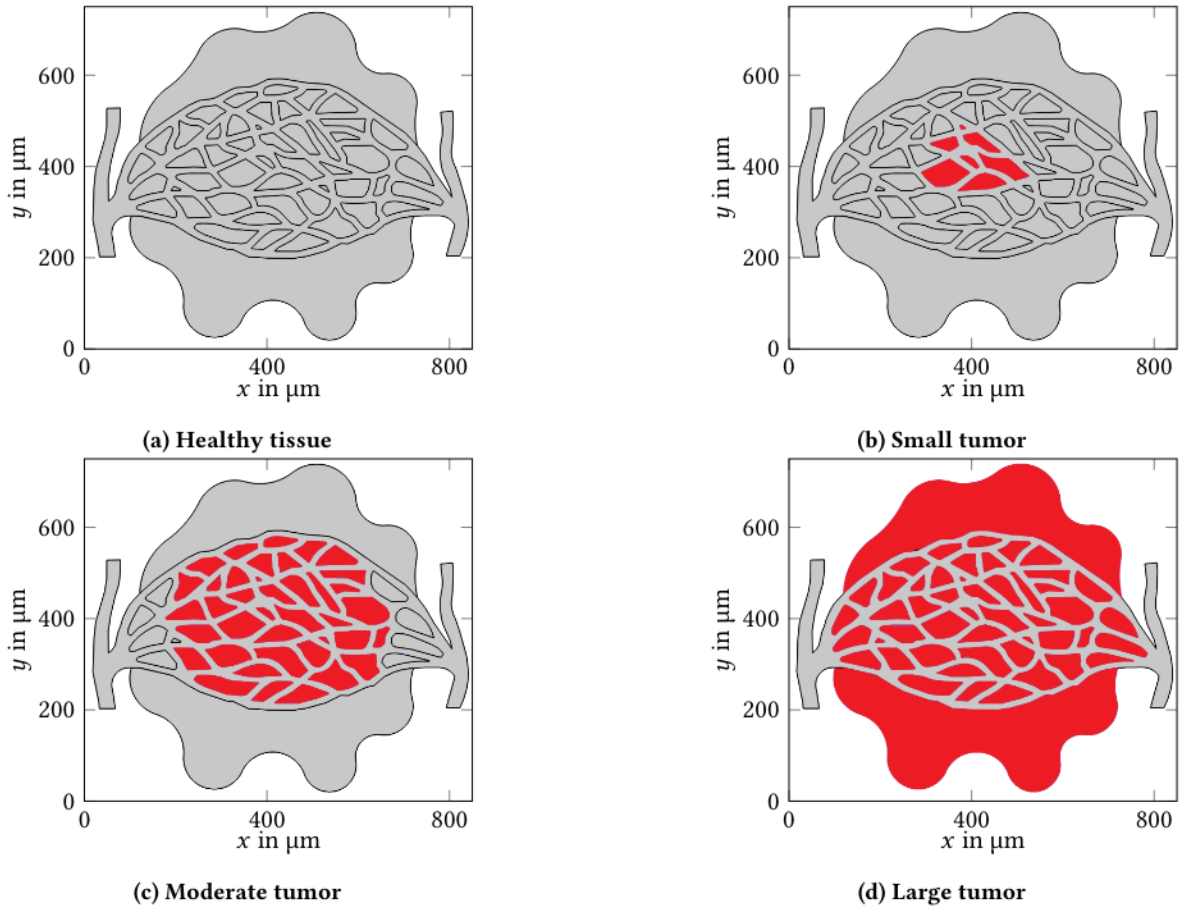

Figure 3: (a) Healthy tissue and sub-millimeter red-colored parts for (b) small, (c) moderate, and (d) large tumor sizes.

[14] Gijung Kim, Min Chul Park, Seonae Jang, Daeyoung Han, Hojun Kim, Wonjune Kim, Honggu Chun, and Sunghoon Kim. 2021. Diffusion-Based Separation of Extracellular Vesicles by Nanoporous Membrane Chip. *Biosensors* 11, 9 (2021), 347.

[15] Roy Koomullil, Behnam Tehrani, Kayla Goliwas, Yong Wang, Selvarangan Ponnazhagan, Joel Berry, and Jessy Deshane. 2021. Computational Simulation of Exosome Transport in Tumor Microenvironment. *Frontiers in medicine* 8 (2021), 643793. https://doi.org/10.3389/fmed.2021.643793

[16] Nandyala Mahesh, Neetu Singh, and Prabal Talukdar. 2022. A mathematical model for understanding nanoparticle biodistribution after intratumoral injection in cancer tumors. *Journal of Drug Delivery Science and Technology* 68 (2022), 103048. https://doi.org/10.1016/j.jddst.2021.103048

[17] Milad Mirzaee and Yanghyo Kim. 2022. Sub-Millimeter Melanoma Skin Cancer Detection: Differentiating Between Healthy and Malignant Tissues Based on Local Specific Absorption Rate. In *2022 IEEE International Symposium on Antennas and Propagation and USNC-URSI Radio Science Meeting (AP-S/URSI)*. IEEE, IEEE, Denver, CO, USA, 351–352.

[18] Bert Müller, Sabrina Lang, Marco Dominietto, Markus Rudin, Georg Schulz, Hans Deyhle, Marco Germann, Franz Pfeiffer, Christian David, and Timm Weitkamp. 2008. High-resolution tomographic imaging of microvessels. In *Developments in X-ray Tomography VI*, Vol. 7078. SPIE, SPIE, San Diego, CA, USA, 89–98.

[19] Max Piffoux, Amanda K. A. Silva, Claire Wilhelm, Florence Gazeau, and David Tareste. 2018. Modification of Extracellular Vesicles by Fusion with Liposomes for the Design of Personalized Biogenic Drug Delivery Systems. *ACS nano* 12 (July 2018), 6830–6842. Issue 7. https://doi.org/10.1021/acsnano.8b02053

[20] Jasmina S Redzic, Agnieszka A Kendrick, Karim Bahmed, Kristin D Dahl, Chad G Pearson, William A Robinson, Steven E Robinson, Michael W Graner, and Elan Z Eisenmesser. 2013. Extracellular vesicles secreted from cancer cell lines stimulate secretion of MMP-9, IL-6, TGF-β1 and EMMPRIN. *PloS one* 8, 8 (2013), e71225.

[21] Hamid Khoshfekr Rudsari, Mohammad Zoofaghari, Martin Damrath, Mladen Veletić, Jacob Bergsland, and Ilangko Balasingham. 2023. Anomalous Diffusion of Extracellular Vesicles in an Extracellular Matrix for Molecular Communication. *IEEE Transactions on Molecular, Biological and Multi-Scale Communications* 9 (2023), 8–12. Issue 1. https://doi.org/10.1109/TMBMC.2023.3240928

[22] Eva Syková and Charles Nicholson. 2008. Diffusion in brain extracellular space. *Physiological reviews* 88 (Oct. 2008), 1277–1340. Issue 4. https://doi.org/10.1152/physrev.00027.2007

[23] Adam Updegrove, Nathan M. Wilson, Jameson Merkow, Hongzhi Lan, Alison L. Marsden, and Shawn C. Shadden. 2017. SimVascular: An Open Source Pipeline for Cardiovascular Simulation. *Annals of Biomedical*

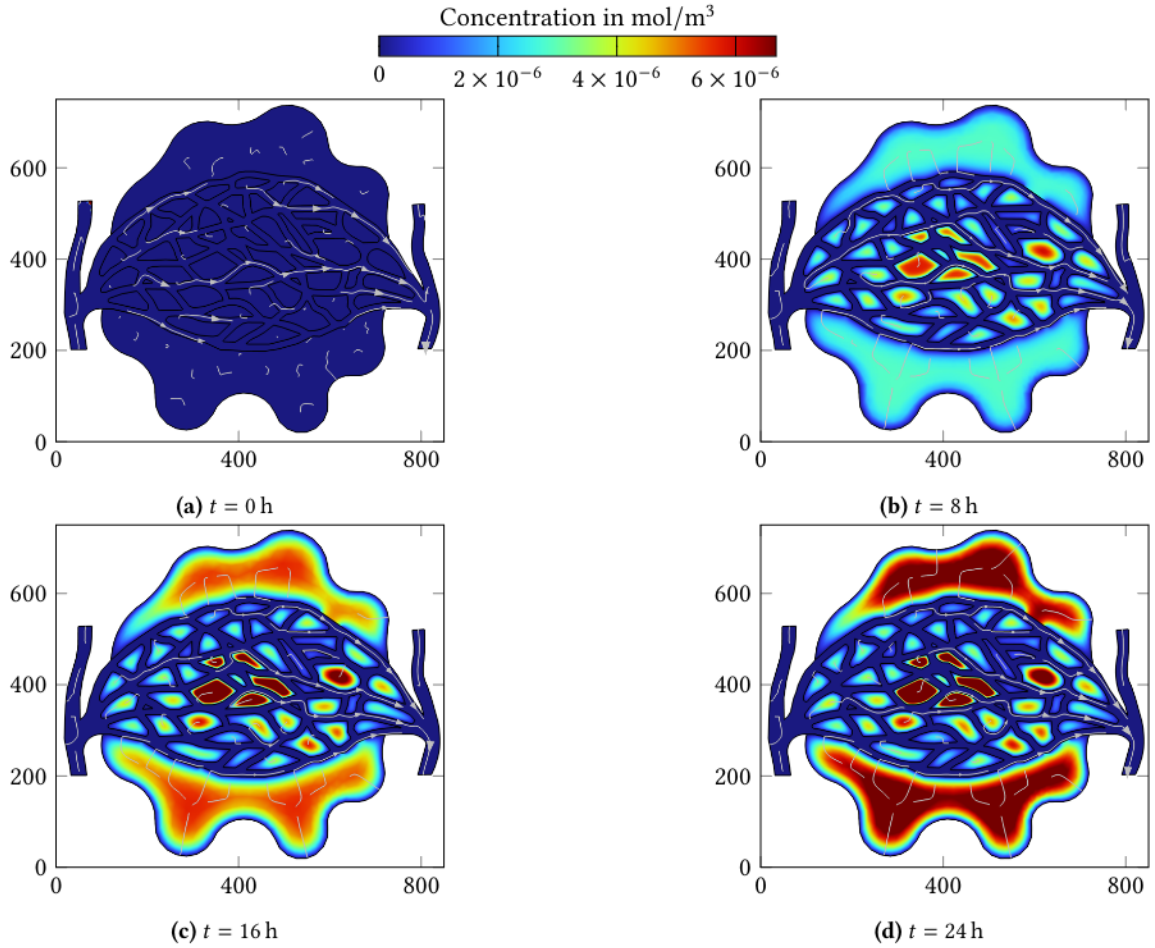

Figure 4: Concentration of EVs inside the tissue and the bloodstream for the small tumor given by Fig. 3b at (a) t=0 h, (b) t=8 h, (c) t=16 h, and (d) t=24 h.

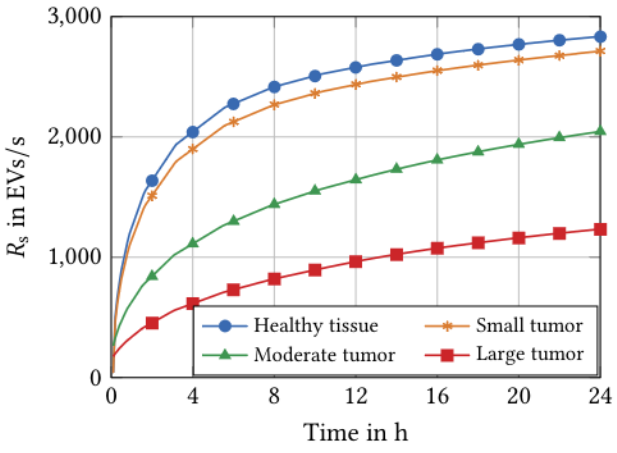

Figure 5: Penetration rate of EVs versus time within the circulatory system for various tumor sizes.

Engineering 45, 3 (2017), 525–541. https://doi.org/10.1007/s10439-016-1762-8

[24] Beatriz Y Salazar Vázquez. 2011. Blood pressure and blood viscosity are not correlated in normal healthy subjects. *Vascular health and risk management* (2011), 1–6.

[25] Mladen Veletić, Michael Taynnan Barros, Ilangko Balasingham, and Sasitharan Balasubramaniam. 2019. A Molecular Communication Model of Exosome-mediated Brain Drug Delivery. In *Proc. ACM Int. Conf. on Nanoscale Computing and Communication (NANOCOM)*. Association for Computing Machinery, Dublin, Ireland, 1–7. https://doi.org/10.1145/3345312.3345478

[26] Liang Wang, Jin Yuan, Hong Jiang, Wentao Yan, Hector R Cintrón-Colón, Victor L Perez, Delia Cabrera DeBuc, William J Feuer, and Jianhua Wang. 2016. Vessel sampling and blood flow velocity distribution with vessel diameter for characterizing the human bulbar conjunctival microvasculature. *Eye & contact lens* 42, 2 (2016), 135.